

Performance Analysis for Multi-layer UAV Networks

Dongsun Kim and Jemin Lee

Department of Information and Communication Engineering (ICE)
Daegu Gyeongbuk Institute of Science and Technology (DGIST), Korea
Email: yidaever@dgist.ac.kr, jmnlee@dgist.ac.kr

Abstract—In this paper, we provide the model of the multi-layer aerial network (MAN), composed unmanned aerial vehicles (UAVs) that distributed in Poisson point process (PPPs) with different densities, floating heights, and transmission power. In our model, we consider the line of sight (LoS) and non-line of sight (NLoS) channels and the probability of forming LoS. We first derive the probability distribution function (PDF) of the main link distance and the Laplace transform of interference of MAN considering strongest average received power-based association. We then analyze the successful transmission probability (STP) of the MAN. We also provide the upper bound of the optimal density that maximizes the STP. Through the numerical results, we show the existence of the optimal height of UAV due to a performance tradeoff caused by the height of the aerial network (AN), and also show the upper bounds of the optimal densities in terms of the STP, which decrease with the height of the ANs.

Index Terms—Stochastic geometry, aerial networks, multi-layer, Poisson point process, association rule, optimal density.

I. INTRODUCTION

Recent developments in the unmanned aerial vehicle (UAV) technology increase payloads capacity, average flight time, and battery capacity that enables the UAV to play an important role in wireless networks. In the area which needs quick deployment of the base station (BS) due to disaster or events, UAVs are expected to act as a temporal BS as well [1]. Furthermore, the data collection from the Internet of Thing (IoT) devices under certain energy constraints can be done by using UAVs [2]. In addition, demands on the data acquisition using UAV in crowd surveillance have arisen [3]. To utilize UAVs for the aforementioned applications and services, the research on the establishment of reliable aerial network (AN) is required.

The UAV based wireless communications has been studied in [4]–[7] after modeling the wireless channel and the mobility, which are different from those of the terrestrial networks. In [4], the pathloss and the channel gain of the link between UAV and ground node are modeled by regression of ray tracing in urban area. Similarly, in [5], the probability that a link forms line of sight (LoS), i.e., the LoS probability, is modeled, which is determined by the angle from the ground, and also proposed the optimal UAV deployment that maximizes the coverage area. In addition, UAV relay networks in cellular networks and device-to-device communications are considered in [6] and [7], respectively. However, the studies

mentioned above have considered only the small number of UAVs, which can show the performance only for the limited scenarios.

Recently, the research on the ANs, which consist of multiple UAVs, is presented in [8]–[10] using stochastic geometry, which is a widely-used tool for randomly distributed nodes [11]. The coexistence of AN and the terrestrial cellular networks is studied by considering the distribution of UAVs as 3-D Poisson point process (PPP) and 2-D PPP in [8] and [10], respectively. The coverage probability of UAV by using binomial point process (BPP)-based distribution is presented in [9]. In addition, [12] studies the multi-tier drone network and shows the downlink spectral efficiency of the network via simulations. However, except for [12], most of these works did not consider the multiple layer structure of ANs, of each layer has UAVs in different heights. In ANs, we can have various types of UAVs with different floating heights and transmission power depending on their hardware constraints [13]. In addition, as the number of UAVs increases, it is required to have the *multiple layer structure* in AN for efficient resource management and reliable coexistence among UAVs. In [12], the multiple layer of ANs is considered, but no performance analysis has been provided.

Therefore, in this paper, we investigate the performance of the multi-layer aerial network (MAN) with various types of UAV. Specifically, the MAN is composed of K layer ANs that have UAVs with different transmission power, spatial densities, and floating heights. Note that the multiple layer structure has been considered for terrestrial networks, which is called as the heterogeneous networks [14]–[16]. However, different to those works, the heights of nodes need to be considered together with the channel model which has the LoS probability determined by the height of node. This leads to new analysis on the interference and the successful transmission probability (STP) of the MAN. Our contribution can be summarized as follows:

- using stochastic geometry, we newly analyze the Laplace transform of interference of MAN by considering different channels for non-line of sight (NLoS) and LoS links with the LoS probability;
- we derive the STP when a ground node selects a UAV with the strongest average received power for communications;

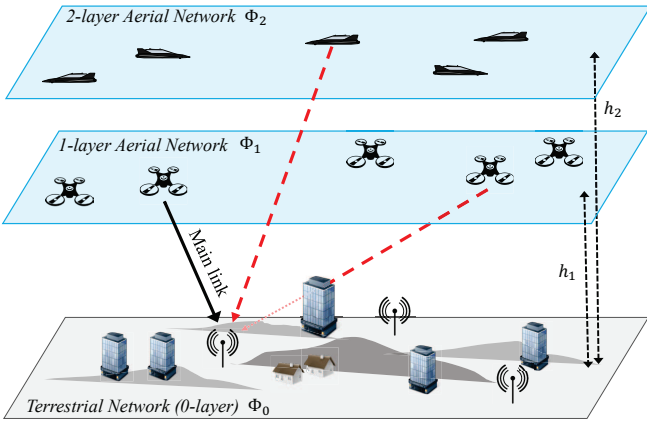


Fig. 1. An example of two layer AN with ground nodes (i.e., 0-layer). The black lines represent the main link from a transmitter to a receiver and red dashed lines represent interference links which comes from other UAVs.

- we provide the upper bounds of the optimal UAV densities of each layer AN that maximize the STP; and
- we show the effects of channel and network parameters on the optimal heights of ANs and the compatibility of the upper bound of optimal densities.

II. SYSTEM MODEL

In this section, we present the system model of MAN with UAV including the network description and the channel model. Furthermore, we describe the association rule which is used to obtain the probability distribution function (PDF) of the main link distance.

A. Multi-layer Aerial Networks

We consider a MAN which consists of K layers of ANs at different altitudes with a terrestrial network as shown in Fig .1. We denote \mathcal{K} as the set of AN layer indexes, i.e., $\mathcal{K} = \{1, \dots, K\}$, and layer 0 as the terrestrial network. We assume UAV in ANs and the ground nodes in the terrestrial network are distributed according to PPPs [11]. Specifically, in the k -layer, the node locations follows a homogeneous PPP Φ_k with density λ_k and they are at the fixed altitude h_k and transmit with the power P_k . Note that the altitude of nodes in the 0-layer (i.e., the terrestrial layer) is $h_0 = 0$ and altitudes of other layers are $h_k > 0$ for $k \in \mathcal{K}$.

In the MAN, we consider the communication from a UAV to a ground node.¹ In the communication with UAVs, we should consider both LoS and NLoS channels since the existence of obstacles (e.g., buildings) between the transmitter and the receiver can be changed with the altitude of UAV. In [5], the probability of forming LoS channel is modeled by a signomial approximation of the probability of having obstructions between transmitter and receiver. When a node

¹Note that our work can be readily extended to multiple scenarios as well such as the communications between UAVs in the same or different layers.

in the k -layer transmits to a ground node, the LoS probability is defined as [5]

$$\rho_k^{(L)}(x) = \frac{1}{1 + a \exp(-b[\sin^{-1}(\frac{h_k}{x}) - a])} \quad (1)$$

where a and b are the parameters related with environments, and x is the link distance between the transmitter and the receiver. From (1), we can see that the LoS probability increases with x which means higher altitude gives higher LoS probability since there will be fewer obstructions. The NLoS probability is then given as $\rho_k^{(N)}(x) = 1 - \rho_k^{(L)}(x)$.

Since each link between a transmitter and a receiver can be in either LoS or NLoS with the probabilities, $\rho_k^{(L)}(x)$ and $\rho_k^{(N)}(x)$, respectively, we can divide a set of the k -layer transmitters into the ones in LoS and the ones in NLoS as $\Phi_k^{(L)}$ and $\Phi_k^{(N)}$, respectively, which are non-homogeneous PPPs. The densities of nodes in $\Phi_k^{(L)}$ and $\Phi_k^{(N)}$ with the distance x from a receiver are, respectively, defined according to the link distance x as $\lambda_k^{(L)}(x) = 2\pi x \lambda_k \rho_k^{(L)}(x)$ and $\lambda_k^{(N)}(x) = 2\pi x \lambda_k - \lambda_k^{(L)}(x)$.

We also consider different channel models for links in LoS and NLoS. The pathloss exponents for LoS and the NLoS links are denoted by $\alpha^{(L)}$ and $\alpha^{(N)}$, respectively, and generally, $2 \leq \alpha^{(L)} \leq \alpha^{(N)} \leq 6$. We consider the Nakagami- m fading for the channels of LoS and the NLoS links, of which channel gains are respectively presented by $G^{(L)} \sim \Gamma(m^{(L)}, \frac{1}{m^{(L)}})$ and $G^{(N)} \sim \Gamma(m^{(N)}, \frac{1}{m^{(N)}})$. Here, we use $m^{(N)} = 1$, which gives Rayleigh fading, i.e., $G^{(N)} \sim \exp(1)$, while $m^{(L)} \geq 1$.

B. Association Rule

In this paper, we assume a receiver connects to the transmitter, which has the strongest average received power described in [17]. This can be applied to the scenario that in the presence of UAV based BSs [1], a user selects a BS to receive its data. Based on the association rule, we can present the selected transmitter's coordinates \mathbf{x}_{main} as

$$\mathbf{x}_{\text{main}} = \arg \max_{\mathbf{x} \in \Phi_k, k \in \mathcal{K}} P_k \|\mathbf{x} - \mathbf{x}_{\text{rec}}\|^{-\alpha_{\mathbf{x}}} \quad (2)$$

where \mathbf{x}_{rec} is the coordinates the receiver is located, and $\alpha_{\mathbf{x}}$ is the pathloss exponent of the link between the transmitter at \mathbf{x} and the receiver.

Based on the association rule above, we can determine the PDF of the distance for *the main link* from a selected transmitter to a receiver. In conventional terrestrial networks, the PDF of main link distance is determined by the transmission power, the pathloss exponent, and the link distance. However, in ANs, we need to additionally consider the LoS/NLoS probabilities for all links to the transmitters. We denote the channel environment by $c \in \text{N, L}$, where $c = \text{N}$ and $c = \text{L}$, respectively, means the LoS and NLoS environments of the link. The PDF of main link distance in c channel condition is presented in following lemma.

Lemma 1: When a transmitter in the j -layer under the channel environment c is selected, the PDF of main link

distance $Y_j^{(c)}$ is given by

$$f_{Y_j^{(c)}}(y) = \frac{f_{V_j^{(c)}}(y)}{\mathcal{A}_j^{(c)}} \prod_{\substack{k \in \mathcal{K}, c_0 \in \{\text{L}, \text{N}\}, \\ (k, c_0) \neq (j, c)}} \bar{F}_{V_k^{(c_0)}} \left(\left(\frac{P_k y^{\alpha^{(c)}}}{P_j} \right)^{\frac{1}{\alpha^{(c_0)}}} \right) \quad (3)$$

where $\mathcal{A}_j^{(c)}$ is association probability given by

$$\mathcal{A}_j^{(c)} = \int_{y>0} f_{V_j^{(c)}}(y) \prod_{\substack{k \in \mathcal{K}, c_0 \in \{\text{L}, \text{N}\}, \\ (k, c_0) \neq (j, c)}} \bar{F}_{V_k^{(c_0)}} \left(\left(\frac{P_k y^{\alpha^{(c)}}}{P_j} \right)^{\frac{1}{\alpha^{(c_0)}}} \right) dy \quad (4)$$

where $V_k^{(c_0)}$ is the distance to the nearest node among the nodes in the k -layer under the channel environment $c_0 \in \{\text{N}, \text{L}\}$, and $\bar{F}_{V_j^{(c_0)}}(v)$ and $f_{V_j^{(c_0)}}(v)$ are the complementary cumulative distribution function (CCDF) and the PDF of $V_j^{(c_0)}$, given by

$$\bar{F}_{V_j^{(c_0)}}(v) = \exp \left[- \int_{h_j}^{\max(v, h_j)} 2\pi \lambda_j x \rho_j^{(c_0)}(x) dx \right] \quad (5)$$

$$f_{V_j^{(c_0)}}(v) = 2\pi \lambda_j v \rho_j^{(c_0)}(v) \exp \left[- \int_{h_j}^v 2\pi \lambda_j x \rho_j^{(c_0)}(x) dx \right] \quad (6)$$

where $f_{V_j^{(c_0)}}$ is 0 when $v < h_j$.

Proof: The cumulative distribution function (CDF) of $V_j^{(c_0)}$ is given by

$$\begin{aligned} F_{V_j^{(c_0)}}(v) &= \mathbb{P} \left(V_j^{(c_0)} \leq v \right) = 1 - \mathbb{P} \left(|\Phi_j^{(c_0)} \cap B(o, v)| = 0 \right) \\ &\stackrel{(a)}{=} 1 - \exp \left[- \int_{h_j}^{\max(v, h_j)} \lambda_j^{(c_0)}(x) dx \right] \end{aligned} \quad (7)$$

where (a) is from the void probability of PPP, and from (7), we have (5) and differentiating (7) with respect to v gives (6). Since the main link have smallest pathloss, probability that main link distance is smaller than y when $\mathbf{x}_{\text{main}} \in \Phi_j^{(c)}$ is given by

$$\begin{aligned} &\mathbb{P} \left(Y_j^{(c_0)} \leq y \cap \text{main link in } j\text{-layer under channel } c \right) \\ &= \int_0^y f_{V_j^{(c)}}(v) \mathbb{P} \left(\mathbf{x}_{\text{main}} \in \Phi_j^{(c)} \cap V_j^{(c)} = v \right) dv \quad (8) \\ &\stackrel{(a)}{=} \int_0^y f_{V_j^{(c)}}(v) \prod_{\substack{k \in \mathcal{K}, c_0 \in \{\text{L}, \text{N}\}, \\ (k, c_0) \neq (j, c)}} \mathbb{P} \left[P_j v^{-\alpha^{(c)}} \geq P_k \left(V_k^{(c_0)} \right)^{-\alpha^{(c_0)}} \right] dv \end{aligned}$$

where (a) from (2). Therefore, we derived the association probability as (4) by $y \rightarrow \infty$. Furthermore, we can derived the PDF of the main link distance as (7). ■

III. INTERFERENCE ANALYSIS AND SUCCESSFULLY TRANSMISSION PROBABILITY

In this section, we analyze the interference free region and the Laplace transform of the interference. Then, we derive the STP of the MAN and the upper bound of the density of AN that maximize the total STP.

A. Interference Free Region and the Laplace Transform

In the MAN, when the j -layer transmitter under the channel environment c is selected, the interference from transmitters in the k -layer under the channel environment c_0 is given by

$$I_k^{(c_0)} = \sum_{\mathbf{x} \in \Phi_k^{(c_0)}} P_k^{(c_0)} (\|\mathbf{x} - \mathbf{x}_{\text{rec}}\|) \quad (9)$$

where $P_k^{(c_0)}$ is the received power from the transmitter which is given by

$$P_k^{(c_0)}(x) = P_k G^{(c_0)} x^{-\alpha^{(c_0)}}. \quad (10)$$

The Laplace transform of the interference is given in the following lemma.

Lemma 2: When a transmitter in the j -layer under the channel environment c with distance d , $\mathbf{x}_j^{(c)}(d)$, is selected, the Laplace transform of the interference from the transmitting nodes in the k -layer under the channel environment c_0 is given by (11), which presented on the top of next page, where $R_{j,k}^{(c,c_0)}(d) = \left(P_k d^{\alpha^{(c)}} / P_j \right)^{1/\alpha^{(c_0)}}$.

Proof: The Laplace transform of the interference is given by

$$\begin{aligned} &\mathcal{L}_{I_k^{(c_0)} | \mathbf{x}_j^{(c)}(d)}(s) \\ &= \mathbb{E}_{\Phi_k^{(c_0)}, G^{(c_0)}} \left[\prod_{\mathbf{x} \in \Phi_k^{(c_0)}} \exp \left(-s P_k G^{(c_0)} x^{-\alpha^{(c_0)}} \right) \middle| \mathbf{x}_j^{(c)}(d) \right] \\ &\stackrel{(a)}{=} \mathbb{E}_{\Phi_k^{(c_0)}} \left[\prod_{\mathbf{x} \in \Phi_k^{(c_0)}} \left(\frac{1}{1 + \frac{s P_k \mathbf{x}^{-\alpha^{(c_0)}}}{m^{(c_0)}}} \right)^{m^{(c_0)}} \middle| \mathbf{x}_j^{(c)}(d) \right]. \end{aligned} \quad (12)$$

Here, we replace $\|\mathbf{x} - \mathbf{x}_{\text{rec}}\|$ with x and (a) is from the expectation over channel $G^{(c_0)}$ which gives the moment-generating function (MGF) of Gamma distribution. Since $\lambda_k^{(c_0)}(x) = 2\pi x \lambda_k \rho_k^{(c_0)}(x)$, the probability generating functional (PGFL) of non-homogeneous PPP needs to be obtained as [11]

$$\begin{aligned} &\mathbb{E} \left[\prod_{\mathbf{x} \in \Phi_k^{(c_0)}} f(\mathbf{x}) \middle| \mathbf{x}_j^{(c)}(d) \right] \\ &= \exp \left(-2\pi \lambda_k \int_{R'}^{\infty} x (1 - f(x)) \rho_k^{(c_0)}(x) dx \right). \end{aligned} \quad (13)$$

In (13), selecting a transmitter in the j -layer under the channel environment c by (2) means there is no interfering node in the k -layer under channel environment c_0 , closer than $R' = \max \left(R_{j,k}^{(c,c_0)}(d), h_k \right)$. Combined with (12) and (13), we obtain the Laplace transform interference under condition $\mathbf{x}_j^{(c)}(d)$ as (11) ■

From Lemma 2, when a transmitter in the j -layer under the channel environment c with main link distance is d is selected, we can obtain the Laplace transform of the sum of the interference and noise as

$$\mathcal{L}_{I | \mathbf{x}_j^{(c)}(d)}(s) = \exp(-s\sigma^2) \prod_{k \in \mathcal{K}, c_0 \in \{\text{L}, \text{N}\}} \mathcal{L}_{I_k^{(c_0)} | \mathbf{x}_j^{(c)}(d)}(s) \quad (14)$$

$$\mathcal{L}_{I_k^{(c_0)}|\mathbf{x}_j^{(c)}(d)}(s) = \exp \left[-2\pi\lambda_k \left\{ \int_{\max(R_{j,k}^{(c,c_0)}(d), h_k)}^{\infty} x \rho_k^{(c_0)}(x) \left(1 - \left(\frac{1}{1 + \frac{sP_k x^{-\alpha(c_0)}}{m^{(c_0)}}} \right)^{m^{(c_0)}} \right) dx \right\} \right] \quad (11)$$

where $\mathcal{I} = \sum_{k \in \mathcal{K}}^{c_0 \in \{L, N\}} I_k^{(c_0)} + \sigma^2$ for the noise power σ^2 .

B. Successful Transmission Probability

We now analyze the STP of MAN in this subsection. When the main link is in the channel environment c with the link distance d , the STP is defined using signal to interference plus noise ratio (SINR) as

$$p_j^{(c)}(d) = \mathbb{P} \left[\text{SINR}_j^{(c)}(d) > \beta \right] \quad (15)$$

where $\text{SINR}_j^{(c)}(d) = P_j^{(c)}(d)/\mathcal{I}$, and β is the target SINR, which is related with the transmission rate. When the association rule in (2) is used, the STP of MAN is presented in the following lemma.

Lemma 3: The STP of the MAN is given by

$$\mathcal{P} = \sum_{j \in \mathcal{K}, c \in \{L, N\}} \int_{h_j}^{\infty} p_j^{(c)}(y) f_{Y_j^{(c)}}(y) \mathcal{A}_j^{(c)} dy \quad (16)$$

where $f_{Y_j^{(c)}}(y)$ and $\mathcal{A}_j^{(c)}$ is in (3) and (4), $p_j^{(c)}(y)$ is presented as

$$p_j^{(c)}(y) = \sum_{n=0}^{m^{(c)}-1} \frac{(-s)^n}{n!} \frac{d^n}{ds^n} \mathcal{L}_{\mathcal{I}|\mathbf{x}_j^{(c)}(y)}(s) \Big|_{s=S_j^{(c)}(y)}, \quad (17)$$

$$S_j^{(c)}(y) = \frac{m^{(c)}\beta}{P_j y^{-\alpha^{(c)}}}, \quad (18)$$

and $\mathcal{L}_{\mathcal{I}|\mathbf{x}_j^{(c)}(y)}(s)$ is in (11).

Proof: From the definition of STP, we have the conditional STP when a transmitter in j -layer under channel environment c is selected with the main link distance j represented as

$$\begin{aligned} p_j^{(c)}(d) &= \mathbb{P} \left[G^{(c)} > \frac{\beta \mathcal{I}}{P_j d^{-\alpha^{(c)}}} \mid \mathbf{x}_j^{(c)}(d) \right] \\ &\stackrel{(a)}{=} \mathbb{E} \left[1 - \frac{1}{\Gamma(m^{(c)})} \gamma \left(m^{(c)}, \frac{m^{(c)}\beta}{P_j d^{-\alpha^{(c)}}} \mathcal{I} \right) \mid \mathbf{x}_j^{(c)}(d) \right] \\ &\stackrel{(b)}{=} \mathbb{E} \left[\sum_{n=0}^{m^{(c)}-1} \frac{(s\mathcal{I})^n}{n!} \exp(-s\mathcal{I}) \mid \mathbf{x}_j^{(c)}(d) \right] \Big|_{s=S_j^{(c)}(d)} \end{aligned} \quad (19)$$

where (a) follows from the Gamma distribution of channel gain and (b) follows from the property of lower incomplete Gamma function. Notice that we derived (18) from (b). Using the property of the following Laplace transform

$$(-\mathcal{I})^n \mathcal{L}_{\mathcal{I}}(s) = \frac{d^n}{ds^n} \mathcal{L}_{\mathcal{I}}(s) \quad (20)$$

we obtain (17). Furthermore, from the PDF and association probability in the Lemma 1, we obtain (16). ■

As shown in (16), it is not possible to present STP in a closed form, so we cannot obtain the optimal densities of

each AN layer that maximize STP. However, in the following corollary, we present the closed-form upper bound of the optimal densities for a special case.

Corollary 1: For the case of $m^{(N)} = m^{(L)} = 1$, when the optimal density of the j -layer AN is λ_j^* , its upper bound is given by

$$\lambda_j^* \leq \lambda_j^b = \frac{1}{2\pi\epsilon_j(\mathcal{S}_j^{(L)}(h_j))} \quad (21)$$

where $\mathcal{S}_j^{(L)}(h_j)$ is in (18), and $\epsilon_j(s)$ is given by

$$\epsilon_j(s) = \int_{h_j}^{\infty} x \left(1 - \frac{\rho_j^{(L)}(x)}{1 + sP_j x^{-\alpha^{(L)}}} - \frac{\rho_j^{(N)}(x)}{1 + sP_j x^{-\alpha^{(N)}}} \right) dx. \quad (22)$$

Proof: See Appendix A. ■

Note that in Corollary 1, the upper bound λ_j^b is only affected by the network parameter of the j -layer AN such as P_j and h_j , but independent with the densities and transmission power of other ANs. Hence, the upper bound of each layer's density in MAN can be determined independently each other. Furthermore, due to the above independency, we can also obtain the upper bound of the total density of MAN as $\lambda_T^b = \sum_{k \in \mathcal{K}} \lambda_k^b$.

IV. NUMERICAL RESULTS

In this section, we present the numerical results to evaluate our analysis on the STP of MAN with single or two layers of ANs under the interference-limited environments. For the numerical results, we use $\beta = 0.7$, $P_k = 1$ for all k , $\alpha^{(L)} = 2.5$, and $\alpha^{(N)} = 3.5$. Except for Fig. 2, $m^{(N)} = 1$ and $m^{(L)} = 1$ are used. Moreover, we $a = 12.4231$ and $b = 0.1202$ are used for the LoS probability, which are determined for the urban area environment in [5].

Fig. 2 shows the STP as a function of the altitude h_1 in single AN for different values of channel coefficient $m^{(L)} = \{1, 3, 20, 100\}$, where $\lambda_1 = 10^{-5}$ [nodes/m²]. Simulation results, obtained from Monte Carlo simulations, are presented by the dashed lines with filled markers, while analysis results for $m^{(L)} = \{1, 3\}$ are presented by the solid lines with unfilled markers. From Fig. 2, we can first see that the simulation results match well with the analysis. We can also see that for all $m^{(L)}$, the STP first increases and then decreases with h_1 . For small h_1 , as the height increases, the LoS channel probability increases, which makes the main link power stronger and results in the higher STP. However, as h_1 keeps increasing, the main link distance also increases, which makes the main link power smaller. As a result, the optimal value of height can be obtained from the tradeoff between the link distance the the LoS probability.

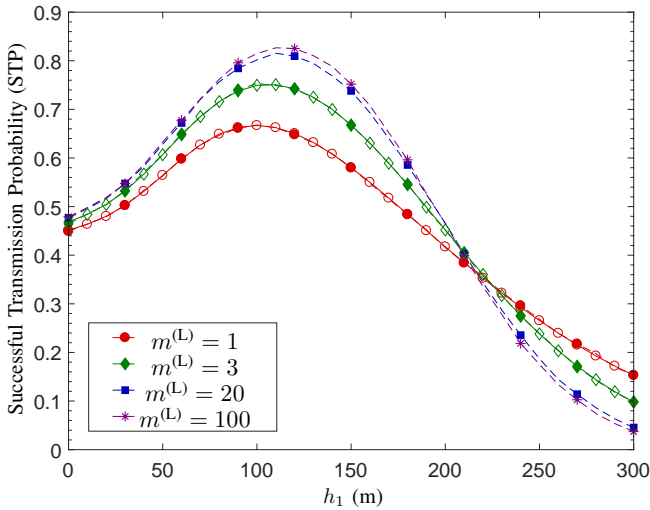


Fig. 2. The STP of single-AN according to the altitude h_1 and the LoS coefficient $m^{(L)}$ when $\lambda_1 = 10^{-5}$.

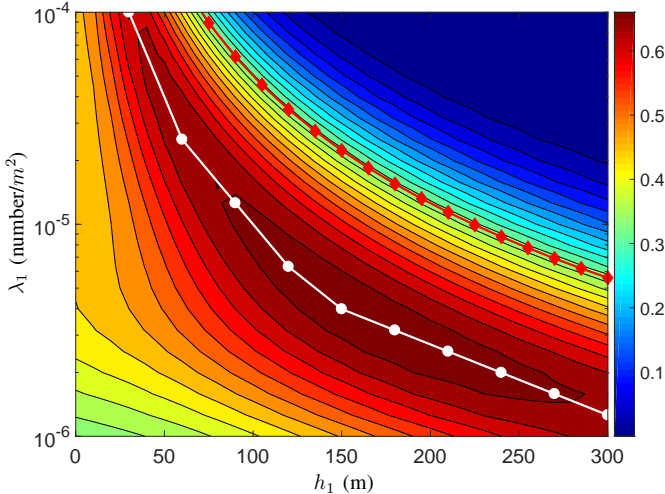


Fig. 3. STP of single AN as functions of the density λ_1 and the height h_1 when $m^{(L)} = 1$. The white line marked by circles represents the optimal density when the height is given and the red line marked by diamonds represents the upper bound of the optimal density.

Furthermore, by comparing the results for different $m^{(L)}$, we can see that for small h_1 , larger LoS coefficient $m^{(L)}$ give higher STP. In smaller h_1 , interference links are more likely to form NLoS, while the main link is more likely to form LoS due to the strongest average received power based association. Hence, smaller variation in main link, i.e., larger $m^{(L)}$, can give higher STP. On the other hands, for large h_1 , $m^{(L)}$ gives different effect since interference links are more likely to form NLoS, which results in lower STP. However, trends of STP according to the height are the same for different $m^{(L)}$. Therefore, we use $m^{(L)} = 1$ in the following numerical results because it can give sufficient insights on the performance of MAN.

Fig. 3 shows the contour of STP as a function of the altitude h_1 and the density λ_1 of UAV in single AN where $m^{(L)} = 1$. We represent the optimal density as a white line with circles and the upper bound of optimal density, obtained from Corollary 1, as a red line with diamonds.

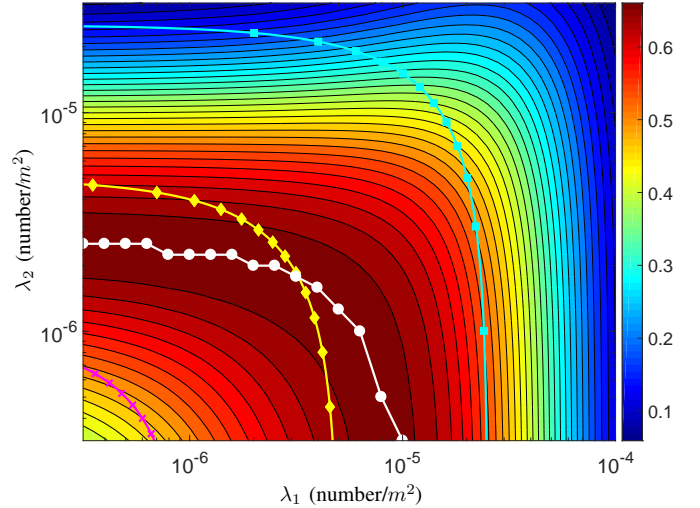


Fig. 4. STP of 2-layer MAN as functions of the density of 1-layer λ_1 and the density of 2-layer λ_2 of UAV when $m^{(L)} = 1$, $h_1 = 100$, and $h_2 = 200$. The white line represents the optimal λ_2 in given λ_1 . The magenta, yellow, and cyan lines with symbols represents the area which have same total density $\lambda_T = \lambda_1 + \lambda_2 = \{10^{-6}, 10^{-5.3}, 10^{-4.6}\}$

By comparing the optimal density and the upper bound of the optimal density, we can notice that the trends according to h_1 are the same. From Fig. 3, we can also see that as the height increases, the optimal density and its upper bound decrease. This is because the number of interfering links in LoS increase with h_1 , so the interference becomes larger.

Fig. 4 shows the contour of STP of MAN with two AN as a function of the density of 1-layer λ_1 and the density of 2-layer λ_2 of UAV, where $m^{(L)} = 1$, $h_1 = 100$, $h_2 = 200$. In this figure, the optimal density of 2-layer λ_2 is presented by a white line with circles. The magenta, yellow, and cyan line with crosses, diamonds, and squares represent the STPs of the MAN that have the total density as $\lambda_T = \lambda_1 + \lambda_2 = \{10^{-6}, 10^{-5.3}, 10^{-4.6}\}$ [nodes/m²], respectively. From (22), the upper bounds of the density of 2-layer is given as $\lambda_2^b = 1.26 \times 10^{-5}$ that coincide with the results, i.e., optimal density of 2-layer $\lambda_2^* \leq \lambda_2^b$.

From Fig. 4, we can also consider the case that the total density of UAV is fixed and we need to allocate portions of UAV density into the two layers. From the colored lines, we can get the relationship of optimal ratio in MAN. Specifically, when the total density of the MAN is small, e.g., the magenta line case, the optimal can be floating all the UAV in the AN layer with higher altitude, i.e., 2-layer AN. However, for the case with large total density of the MAN, e.g., the cyan line case, floating all the UAV in the AN layer with lower altitude, i.e., 1-layer AN, can achieve the highest STP. In other cases, from the result with yellow line, we can see that floating UAVs in both layers with proper densities can be better.

V. CONCLUSION

This paper model the MAN which is wireless networks consist of multi-layers of UAVs that distributed in PPP with different densities, heights, and powers. We consider LoS and

NLoS channel and the strongest transmitter association for the AN. Our approach is to derive the PDF of the main link distance and the Laplace transform of the interference for the STP analysis. By analyzing the STP, we show that each AN in the MAN have the upper bound of optimal density which is given by the function of the height and power of corresponding AN. In addition, our numerical results show the tradeoff caused by height of the AN, affection of LoS coefficient, significance of the upper bound of the optimal density, and optimal densities and optimal ratio of densities in the 2-layer MAN. Specially, our results show higher altitude AN have sparser optimal density and show that the optimal ratio of densities in the 2-layer MAN is changed with the total density of the MAN.

APPENDIX

A. Proof of Corollary 1

From Lemma 3, the STP can be represented by

$$\mathcal{P} = \sum_{j \in \mathcal{K}} \int_{h_j}^{\infty} \left(\varphi_j^{(L)}(y) + \varphi_j^{(N)}(y) \right) dy \quad (23)$$

where $\varphi_j^{(c)}(y)$ is given by

$$\begin{aligned} \varphi_j^{(c)}(y) &= p_j^{(c)}(y) f_{Y_j^{(c)}}(y) \\ &= 2\pi \rho_j^{(c)}(y) \lambda_j y \exp \left[-2\pi \sum_{k \in \mathcal{K}} \lambda_k \phi_{j,k}^{(c)}(y, \mathcal{S}_j^{(c)}(y)) \right] \end{aligned} \quad (24)$$

where $\phi_{j,k}^{(c)}(y, s)$ is given by

$$\begin{aligned} \phi_{j,k}^{(c)}(y, s) &= \sum_{c_0 \in \{L, N\}} \left[\int_{h_k}^{R'} x \rho_k^{(c_0)}(x) dx + \right. \\ &\quad \left. \int_{R'}^{\infty} x \rho_k^{(c_0)}(x) \left(1 - \frac{1}{1 + s P_k x^{-\alpha^{(c_0)}}} \right) dx \right]. \end{aligned} \quad (25)$$

where $R' = \max(R_{j,k}^{(c,c_0)}(y), h_k)$. Notice that $\phi_{j,k}^{(c)}(y, s)$ is increase with y and s . In addition, we can derive the differential of the total STP with density λ_j as

$$\frac{\partial}{\partial \lambda_j} \mathcal{P} = \sum_{k \in \mathcal{K}} \int_{h_k}^{\infty} \frac{\partial}{\partial \lambda_j} \left(\varphi_k^{(L)}(y) + \varphi_k^{(N)}(y) \right) dy \quad (26)$$

where components inside the integral are given by

$$\frac{\partial}{\partial \lambda_j} \varphi_j^{(c)}(y) = \frac{\varphi_j^{(c)}(y)}{\lambda_j} \left(1 - 2\pi \lambda_j \phi_{j,j}^{(c)}(y, \mathcal{S}_j^{(c)}(y)) \right) \quad (27)$$

$$\frac{\partial}{\partial \lambda_j} \varphi_{j'}^{(c)}(y) = \varphi_{j'}^{(c)}(y) \left(-2\pi \phi_{j',j}^{(c)}(y, \mathcal{S}_j^{(c)}(y)) \right) \quad (28)$$

where j' used to represent $j' \neq j$. Notice that (27) is differential of the STP when main link is j -layer. On the other hand, (28) is differente with λ_j for the STP when main link is not j -layer, hence the STP always decrease with λ_k .

Since the total STP and the differential is not closed form, which makes hard to find the optimal densities, we derive range of λ_j that makes differential of STP negative to derive the upper bound of optimal λ_j . In, (27) and (28), $\varphi_j^{(c)}(y)$ and

λ_j is positive for all domain. Hence, if following inequality holds, the total STP decrease with λ_j .

$$\max_{y,c} \left[\frac{1}{2\pi \phi_{j,j}^{(c)}(y, \mathcal{S}_j^{(c)}(y))} \right] \leq \lambda_j \quad (29)$$

Furthermore, as $\phi_{j,j}^{(c)}(y, s)$ is increase with y and s , we can put the minimum value of y and s which gives

$$\phi_{j,j}^{(L)}(h_j, \mathcal{S}_j^{(L)}(h_j)) = \epsilon_j \left(\mathcal{S}_j^{(L)}(h_j) \right). \quad (30)$$

Hence, the upper bound of optimal density is given by (22).

REFERENCES

- [1] Y. Zeng, R. Zhang, and T. J. Lim, "Wireless communications with unmanned aerial vehicles: opportunities and challenges," *IEEE Commun. Mag.*, vol. 54, no. 5, pp. 36–42, May 2016.
- [2] H. Zanjie, N. Hiroki, K. Nei, O. Fumie, M. Ryu, and Z. Baohua, "Resource allocation for data gathering in UAV-aided wireless sensor networks," in *IEEE Conf. on Network Infrastructure and Digital Content*. IEEE, Jan. 2014, pp. 11–16.
- [3] N. H. Motlagh, M. Bagaa, and T. Taleb, "UAV-based IoT platform: A crowd surveillance use case," *IEEE Commun. Mag.*, vol. 55, no. 2, pp. 128–134, May 2017.
- [4] A. Al-Hourani, S. Kandeepan, and A. Jamalipour, "Modeling air-to-ground path loss for low altitude platforms in urban environments," in *Proc. IEEE Global Telecomm. Conf.*, Austin, TX, Feb. 2014, pp. 2898–2904.
- [5] A. Al-Hourani, S. Kandeepan, and S. Lardner, "Optimal LAP altitude for maximum coverage," *IEEE Wireless Commun. Lett.*, vol. 3, no. 6, pp. 569–572, Jul. 2014.
- [6] W. Guo, C. Devine, and S. Wang, "Performance analysis of micro unmanned airborne communication relays for cellular networks," in *IEEE International Symposium on. Communication Systems, Networks & Digital Signal Processing*. IEEE, 2014, pp. 658–663.
- [7] M. Mozaffari, W. Saad, M. Bennis, and M. Debbah, "Unmanned aerial vehicle with underlaid device-to-device communications: Performance and tradeoffs," *IEEE Trans. Wireless Commun.*, vol. 15, no. 6, pp. 3949–3963, Feb. 2016.
- [8] C. Zhang and W. Zhang, "Spectrum sharing in drone small cells," in *Proc. IEEE Global Telecomm. Conf.*, Washington, DC, Feb. 2016, pp. 1–6.
- [9] V. V. Chetlur and H. S. Dhillon, "Downlink coverage analysis for a finite 3-d wireless network of unmanned aerial vehicles," *IEEE Trans. Commun.*, vol. 65, no. 10, pp. 4543–4558, Jul. 2017.
- [10] M. M. Azari, F. Rosas, A. Chiumento, and S. Pollin, "Coexistence of terrestrial and aerial users in cellular networks," *arXiv preprint arXiv:1710.03103*, Oct. 2017. [Online]. Available: <https://arxiv.org/pdf/1710.03103.pdf>
- [11] M. Haenggi and R. K. Ganti, "Interference in large wireless networks," *Foundations and Trends in Networking*, vol. 3, no. 2, pp. 127–248, 2008.
- [12] S. Sekander, H. Tabassum, and E. Hossain, "Multi-tier drone architecture for 5G/B5G cellular networks: Challenges, trends, and prospects," *IEEE Commun. Mag.*, vol. 56, no. 3, pp. 96–103, Mar. 2018.
- [13] S. Chandrasekharan, K. Gomez, A. Al-Hourani, S. Kandeepan, T. Rasheed, L. Goratti, L. Reynaud, D. Grace, I. Bucaille, T. Wirth *et al.*, "Designing and implementing future aerial communication networks," *IEEE Commun. Mag.*, vol. 54, no. 5, pp. 26–34, May 2016.
- [14] S. Singh, H. S. Dhillon, and J. G. Andrews, "Offloading in heterogeneous networks: Modeling, analysis, and design insights," *IEEE Trans. Wireless Commun.*, vol. 12, no. 5, pp. 2484–2497, Apr. 2013.
- [15] H. S. Dhillon, R. K. Ganti, F. Baccelli, and J. G. Andrews, "Modeling and analysis of K-tier downlink heterogeneous cellular networks," *IEEE J. Sel. Areas Commun.*, vol. 30, no. 3, pp. 550–560, Apr. 2012.
- [16] Q. Zhang, H. H. Yang, T. Q. Quek, and J. Lee, "Heterogeneous cellular networks with los and nlos transmissions—the role of massive mimo and small cells," *IEEE Trans. Wireless Commun.*, vol. 16, no. 12, pp. 7996–8010, Sep. 2017.
- [17] H. Cho, C. Liu, J. Lee, T. Noh, and T. Q. Quek, "Impact of elevated base stations on the ultra-dense networks," *IEEE Commun. Lett.*, Apr. 2018.